Inorganic Chemistry

Article

pubs.acs.org/IC

From Serendipity to Rational Design: Tuning the Blue Trigonal Bipyramidal Mn^{3+} Chromophore to Violet and Purple through Application of Chemical Pressure

Jun Li,[†] Simon Lorger,[†] Judith K. Stalick,[‡] Arthur W. Sleight,[†] and M. A. Subramanian*[,†]

[†]Department of Chemistry, Oregon State University, Corvallis, Oregon 97331, United States

[‡]NIST Center for Neutron Research, National Institute of Standards and Technology, 100 Bureau Drive, Gaithersburg, Maryland 20899, United States

Supporting Information

ABSTRACT: We recently reported that an allowed d−d transition of trigonal bipyramidal (TBP) Mn^{3+} is responsible for the bright blue color in the $YIn_{1-x}Mn_xO_3$ solid solution. The crystal field splitting between a′(d_{z^2}) and e′($d_{x^2-y^2}$, d_{xy}) energy levels is very sensitive to the apical Mn−O distance. We therefore applied chemical pressure to compress the apical Mn−O distance in $YIn_{1-x}Mn_xO_3$, move the allowed d−d transition to higher energy, and thereby tune the color from blue to violet/purple. This was accomplished by substituting smaller cations such as Ti^{4+}/Zn^{2+} and Al^{3+} onto the TBP In/Mn site, which yielded novel violet/purple phases. The general formula is $YIn_{1-x-2y-z}Mn_xTi_yZn_yAl_zO_3$ (x = 0.005−0.2, y = 0.1−0.4, and $z \leq 0.1$), where the color darkens with the increasing amount of Mn. Higher y or small additions of Al provide a more reddish hue to the resulting purple colors. Substituting other rare earth cations for Y has little impact on color. Crystal structure analysis by neutron powder diffraction confirms a shorter apical Mn−O distance compared with that in the blue $YIn_{1-x}Mn_xO_3$. Magnetic susceptibility measurements verify the 3+ oxidation state for Mn. Diffuse reflection spectra were obtained over the wavelength region 200−2500 nm. All samples show excellent near-infrared reflectance comparable to that of commercial TiO_2, making them ideal for cool pigment applications such as energy efficient roofs of buildings and cars where reducing solar heat to save energy is desired. In a comparison with commercial purple pigments, such as $Co_3(PO_4)_2$, our pigments are much more thermally stable and chemically inert, and are neither toxic nor carcinogenic.

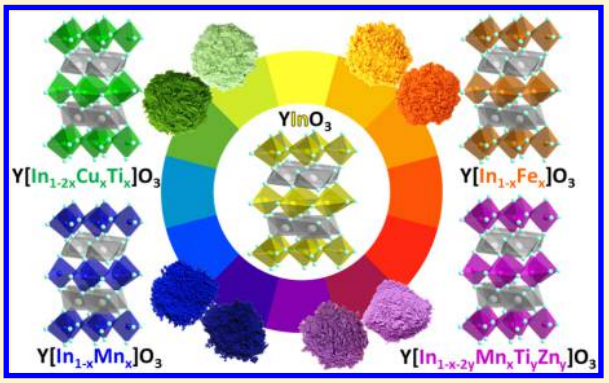

INTRODUCTION

Inorganic pigments are generally more stable than organic pigments. However, traditional blue inorganic pigments have significant stability issues. From the earliest Egyptian blue ($CaCuSi_4O_{10}$) and Chinese Han blue ($BaCuSi_4O_{10}$) to the currently used cobalt blue ($CoAl_2O_4$) and ultramarine ($Na_7Al_6Si_6O_{24}S_3$), inorganic blue pigments all suffer from environmental and/or durability issues. The recent discovery of an intense bright blue color in the $YIn_{1-x}Mn_xO_3$ solid solution has attracted tremendous attention from both the academic and commercial communities.[1−4] This was the first report on the synthesis of oxides with the blue chromophore based on a Mn^{3+} ion in trigonal bipyramidal (TBP) coordination. These new oxides surpass the existing synthetic blue pigments in many aspects: They have brighter color, higher stability, better near-infrared (NIR) reflectance, and they are more environmentally benign. They are now considered as the new Blue Standard.[4]

The discovery of the Y(In, Mn)O_3 blue opened up a new field of research: rational design of novel inorganic pigments through cation substitution into the TBP sites of the host oxides. The hexagonal structure (Figure 1) of $YInO_3$ and $YMnO_3$ can be described as alternating layers of edge-shared YO_6 octahedra and corner-shared MO_5 trigonal bipyramids (M = In, Mn). A complete $YIn_{1-x}Mn_xO_3$ solid solution could be prepared despite the size mismatch between In^{3+} and Mn^{3+} due to the similar In−O and Mn−O basal-plane distances in isostructural $YInO_3$ and $YMnO_3$. We have been able to create a "rainbow" of colors through rational design as shown in Figure 2. Starting from the hexagonal parent compound $YInO_3$, substituting a small amount of iron for indium produces intense orange colors, and replacing some or all indium with titanium and copper makes green colors.[5,6] By replacing some In^{3+} in Y(In, Mn)O_3 with equal amounts of Ti and Zn, we now report a range of violet to purple colors (Figures 1 and 2).

Violet and purple are located between blue and red in the traditional color wheel used by painters, with violet closer to blue and purple closer to red. Historically, they have long been

Received: July 8, 2016
Published: September 13, 2016

DOI: 10.1021/acs.inorgchem.6b01639
Inorg. Chem. 2016, 55, 9798−9804

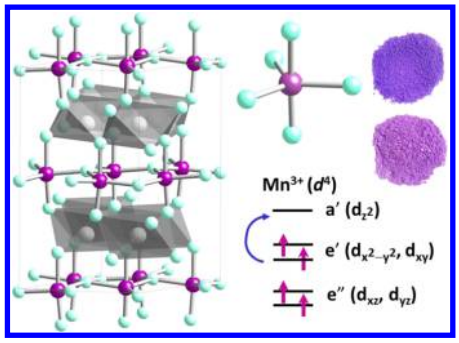

Figure 1. Hexagonal structure of YMO_3 showing alternating layers of corner-shared MO_5 trigonal bipyramids and edge-shared YO_6 octahedra (M = In/Mn/Ti/Zn/Al, purple spheres; O, cyan spheres; Y, gray spheres). Schematic energy levels for the spin-up Mn^{3+} 3d orbitals in trigonal bipyramidal coordination are shown. Transitions from e′ to a′ are formally dipole-allowed in this symmetry.

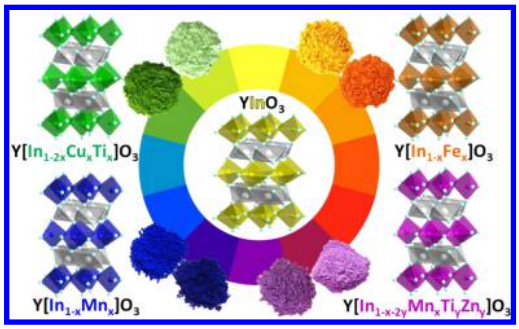

Figure 2. A range of colors can be created through TBP site substitutions in hexagonal $YInO_3$.

associated with royalty, aristocracy, piety, and faith. The use of inorganic violet and purple pigments dates back to 25000 BC when dark violet color was applied for the Pech Merle prehistoric cave paintings in France.[7] These earliest pigments for violet and purple were made by grinding manganese minerals and hematite (Fe_2O_3) into fine powders. Chinese Han purple ($BaCuSi_2O_6$), the first synthetic purple pigment, was found in some murals from Eastern Han tombs of ancient China more than 2000 years old.[8,9] The violet and purple colors utilized by medieval artists were actually created by combining blue azurite ($Cu_3(CO_3)_2(OH)_2$) or lapis-lazuli ($(Na,Ca)_8(AlSiO_4)_6(S,SO_4,Cl,OH)_{1-2}$) with red ochre ($Fe_2O_3$), cinnabar (HgS), or minium (Pb_3O_4).[7] As a variant of the synthetic ultramarine blue ($Na_7Al_6Si_6O_{24}S_3$), ultramarine violet ($Na_{6-10}Al_6Si_6O_{24}S_{2-4}$) did not make its appearance until the early 19th century.[10] Cobalt violet or cobalt(II) phosphate $Co_3(PO_4)_2$ and cobalt(II) arsenate $Co_3(AsO_4)_2$ were first manufactured in 1859 by mixing a soluble cobalt salt with sodium phosphate in aqueous solution.[11] Manganese violet, ammonium manganese(III) pyrophosphate ($NH_4MnP_2O_7$), was developed in 1868 by E. Leykauf and was used as a pigment since the 1890s.[12] Currently, manganese violet and cobalt violet (phosphate only) are still commonly used pigments, along with ultramarine violet and Han purple. Han purple and ultramarine violet are chemically and thermally unstable.[8,13] Manganese violet decomposes around 300 °C, and cobalt violet is subject to steadily increasing environmental regulations worldwide.

Crystals of $YMn_{1-x}Ga_xO_3$ ($x \leq 0.5$) grown by a floating zone technique have been studied for ferroelectric properties, but optical data were not reported.[14] Inspired by the success of intense $Y(In,Mn)O_3$ blue, Tamilarasan et al. reported a series of metastable purple oxides, $YGa_{1-x}Mn_xO_3$,[15] that were prepared by a sol−gel method.[16] We have thoroughly studied the hexagonal $YAlO_3$−$YMnO_3$ solid solution synthesized by the same method and concluded that the compound long assumed to be a hexagonal form of $YAlO_3$ is actually an oxycarbonate with the ideal composition $Y_3Al_3O_8CO_3$.[17] Upon heating in air, this compound transforms to $YAlO_3$ with the perovskite structure, liberating CO_2. The presence of carbonate in citrate-prepared $Y_3Ga_3O_{9-x}(CO_3)_x$ was also confirmed by IR data, and the cell edge analysis suggested an even higher carbonate concentration in the citrate-prepared hexagonal "$RGaO_3$" phases (R = La, Pr, Nd, Sm, or Eu) than that in "$YGaO_3$".[17] Bluish-purple or violet colors can also be produced by introducing Mn^{3+} into the TBP sites of $YbFe_2O_4$-related structures.[18] Our work has motivated others to search for the TBP Mn^{3+} chromophore in different structures.[19,20]

EXPERIMENTAL SECTION

Polycrystalline samples were prepared by conventional solid state synthesis. Stoichiometric amounts of Y_2O_3 (Nucor Research Chemicals 99.9%), In_2O_3 (Aldrich, 99.99%), Mn_2O_3 (Sigma-Aldrich 99%), TiO_2 (JMC 99.99%), ZnO (Sigma-Aldrich, 99.9%, 99.99%), Al_2O_3 (Cerac 99.99%), and Ga_2O_3 (Aldrich 99.99%) were weighed and thoroughly ground using an agate mortar and pestle. The mixed powders were pressed into pellets and calcined at 1200 °C for 12 h in air, and then reground, pelleted, and heated at 1300 °C for one or two more times. Powders of Y_2O_3 and Ga_2O_3 were dried at 850 °C overnight before weighing in order to remove any moisture and carbonate content.

X-ray powder diffraction (XRD) patterns were obtained with a Rigaku MiniFlex II diffractometer using Cu Kα radiation and a graphite monochromator on the diffracted beam. Silicon powder was used as an internal standard to ensure accurate determination of unit cell dimensions. Powder neutron diffraction data were collected on the 32-counter high-resolution diffractometer BT-1 at the Center for Neutron Research at the National Institute of Standards and Technology. A Cu(311) monochromator, yielding a wavelength of 1.5403(2) Å, was employed. Collimation of 15′ of arc was used before the monochromator, 20′ before the sample, and 7′ before the detectors. The samples (≈10 g) were loaded into vanadium containers 15.6 mm in diameter and 50 mm in length. Data were collected at room temperature over a 2θ range 3−167°. Structural refinements of XRD and neutron data were performed using GSAS-EXPGUI software.[21,22] Bond-valence analysis made use of the bond-valence calculator.[23]

A Konica Minolta CM-700d spectrophotometer (Standard illuminant D65) was chosen to measure L^*, a^*, and b^* color coordinates. Diffuse reflectance spectra of the powder samples were determined in the region 200−1150 nm using a homemade UV−vis spectrophotometer with a DH-2000-BAL deuterium-halogen light source. The diffuse light reflected by the powders was collected with a bifurcated fiber optic wire that runs from the light source to the sample and then to the spectrophotometer. MgO was used as a reference for pure white. The data were transformed into absorbance using the Kubelka−Munk function.[24] Near-infrared (NIR) reflectance data (up to 2500 nm) were collected using a Jasco V-670 spectrophotometer.

Zero field cooled (ZFC) dc magnetic data were measured with a Quantum Design Physical Property Measurement System (PPMS) using the ACMS mode with a magnetic field of 0.50 T from 5 to 300 K. Inverse magnetic susceptibility data were fit to the Curie−Weiss law with diamagnetic corrections applied.[25]

RESULTS AND DISCUSSION

Starting from the composition $YIn_{1-x}Mn_xO_3$ with low Mn content ($x \leq 0.2$), the intense blue color was tuned to various

DOI: 10.1021/acs.inorgchem.6b01639
Inorg. Chem. 2016, 55, 9798−9804

shades of violet and purple colors by substituting different amounts of Ti/Zn for In (Figure 3). At a fixed amount of Mn,

Figure 3. Tuning the color from blue to violet and purple through TBP site substitution. The general formula of the selected compositions is $YIn_{1-x-2y-z}Mn_xTi_yZn_yAl_zO_3$.

the purple color turns more reddish with increasing Ti/Zn substitution. The same shift in color occurs when small amounts of Al are added in addition to the Ti/Zn. Substitutions for Y were attempted as well with Ca and rare earth elements (RE = La, Nd, Gd, Dy, Ho, Er, Eu, Yb, Sc), but there was little impact on the color. The same substitutions with Ti/Zn/Al in other hexagonal RE(In, Mn)O_3 hosts (RE = Dy, Ho, Er) produce similar violet and purple colors, although for samples with high Mn concentration, replacing Y with other rare earths made the dark colors become somewhat lighter. The violet to purple samples of $YIn_{1-x-2y-z}Mn_xTi_yZn_yAl_zO_3$ (x = 0.005−0.2, y = 0.1−0.4, z = 0−0.1) were synthesized phase pure up to y = 0.3 and z = 0.1. The y = 0.4 sample contained small amounts of Y_2O_3, In_2O_3, and Zn_2TiO_4 impurities. The sample color darkens as Mn content increases, becoming very dark when x is above 0.2. The XRD powder patterns are shown in Figure 4

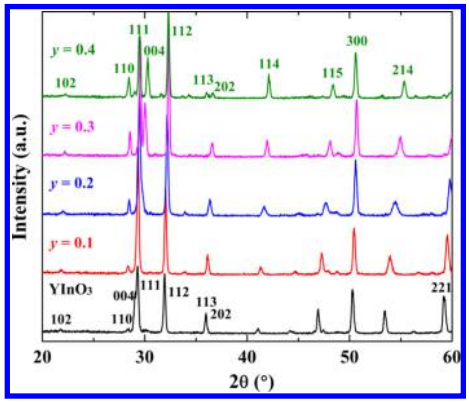

Figure 4. XRD patterns of $YIn_{1-x-2y}Mn_xTi_yZn_yO_3$ (x = 0.05 and y = 0.1−0.4). Major *hkl* reflections are labeled for clarity.

using x = 0.05 as an example. All patterns show a weak peak indicating the 102 reflection that arises from the ferrielectric structure with space group $P6_3cm$. With increasing amounts of Ti and Zn, a shift to higher 2θ angles is observed for most of the diffraction peaks, especially the (004) peak. The very small shifts for the (110) and (300) peaks indicate that the lattice contraction is primarily along the c axis.

Unit cell parameters versus composition are shown in Figure 5 and Supporting Information Figure S1. Cell edges a, c, c/a

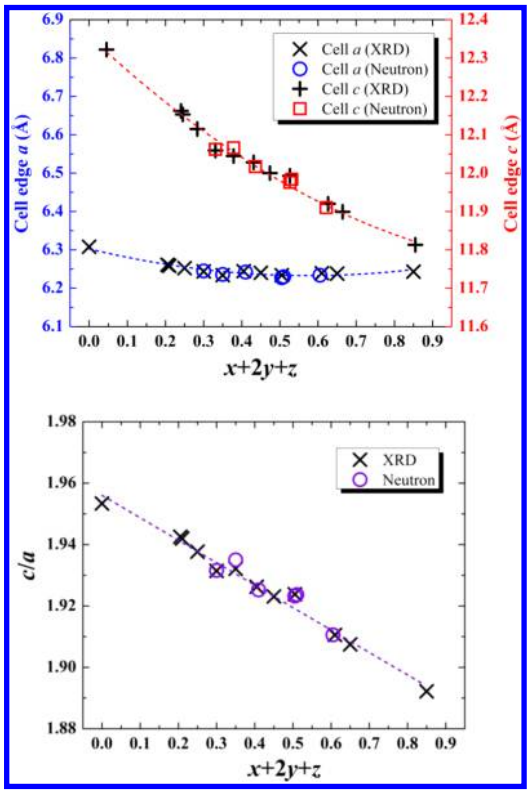

Figure 5. Unit cell dimensions a and c (top) and the c/a ratio (bottom) for the solid solution with a composition of $YIn_{1-x-2y-z}Mn_xTi_yZn_yAl_zO_3$. The value of ($x$ + 2y + z) is the total TBP site substitution for In. Both X-ray and neutron diffraction data are displayed. Dashed lines are drawn to guide the eye. Estimated uncertainties are smaller than the plotted point size.

ratio and cell volume all decrease with increasing substitution due to smaller 3+ ionic radii of Mn/Ti/Zn/Al compared with that of In, which confirms the formation of the solid solution. This figure shows that the chemical pressure resulting from these substitutions is directed primarily along the c axis and impacts the axial TBP distances much more than the basal distances. Like the case of blue Y(In,Mn)O_3 phases, we attribute this miscibility to the similar In−O and M−O (M = Mn, Ti, Zn, Al) basal-plane distances in hexagonal $YIn_{1-x}M_xO_3$.[1] The large size difference between In^{3+} and M^{3+} is manifested only in the apical distances. Similar basal-plane bond distances lead to a weak variation of cell edge a across the solid solution series, while cell edge c, c/a ratio, and cell volume change dramatically with substitution as a result of the decreasing apical M−O distances. The slight negative deviation from linear behavior is likely associated with the tilt angle of the basal-plane triangles.

The structure refinements were based on acentric space group $P6_3cm$ using neutron powder diffraction data. The results are shown in Figure 6 and Supporting Information (Figures S2−S3 and CIF files). The weighted R-factor and χ^2 are 4.5−6.9% and 1.0−1.7, respectively. A typical Rietveld fit is shown in Supporting Information Figure S2 using $YIn_{0.7}Mn_{0.1}Ti_{0.1}Zn_{0.1}O_3$ as an example. Most of our refinements assumed that all TBP cations had the same atomic coordinates. We found that for a simple system like blue $YIn_{0.8}Mn_{0.2}O_3$ we could

DOI: 10.1021/acs.inorgchem.6b01639
Inorg. Chem. 2016, 55, 9798−9804

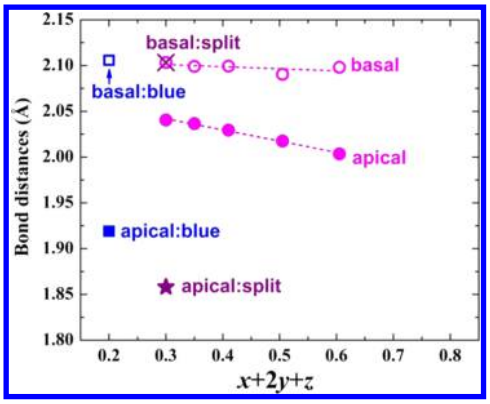

Figure 6. Average bond distances of purple $YIn_{1-x-2y-z}Mn_xTi_yZn_yAl_zO_3$ and blue $YIn_{0.8}Mn_{0.2}O_3$ samples. Open and filled circles are distances refined for purple samples without local relaxation. The cross sign and star (for purple) and the open and filled squares (for blue) are distances refined with split sites for In and Mn and two apical oxygens. The value of $(x + 2y + z)$ is the total TBP site substitution for In. Estimated uncertainties are smaller than the plotted point size.

refine In and Mn positions separately using neutron diffraction data, and refine as well the separate positions for the apical O atoms associated with In and Mn.[26] Such an approach becomes much more challenging for the purple Y(In, Mn, Ti, Zn, Al)O_3 compositions with relatively low Mn content. A split model was, however, successful for $YIn_{0.7}Mn_{0.1}Ti_{0.1}Zn_{0.1}O_3$. This was accomplished by refining the positions of Mn and its apical oxygens separately, leaving In, Ti, Zn, and Al at one site with occupancies fixed according to the nominal composition. Such a refinement is facilitated by the fact that Mn is the only atom in the structure with a negative scattering length.

Figure 6 displays a clear contraction of the apical bond distances with increasing substitution and a minor change in the basal-plane distances. Without allowing local relaxation for Mn, the average apical Mn−O distance is refined to be 2.04 Å, but it becomes much shorter (1.86 Å) when refined with a split model. The same distance is 1.92 Å for blue $YIn_{0.8}Mn_{0.2}O_3$ refined with local relaxation for Mn, indicating a decreasing apical Mn−O bond distance going from blue to purple.[26] The actual difference between apical Mn−O distances of blue and purple samples might be even bigger if local relaxation could be applied for all the TBP cations of the purple samples, given the fact that Shannon radii (Å) for these cations in 5-fold coordination are Mn^{3+} (0.58), Ti^{4+} (0.51), Zn^{2+} (0.68), Al^{3+} (0.48), and In^{3+} (0.723, estimated from the reported $YInO_3$ structure).[27,28]

The decrease in apical Mn−O bond distance is presumably responsible for the color shift from blue to purple since the energy of the d_{z^2} state relative to the valence band maximum is determined by the Mn−O apical bond length (Figure 1). More precisely, the crystal field splitting for Mn^{3+} is related to the ratio of the apical and basal-plane Mn−O distances. Since the apical distances vary much more than the basal-plane distances, it is primarily the apical Mn−O distances that correlate with the position of the allowed d−d transition. To accommodate the larger In−O apical distances, the O−In(M)−O bond angle for the apical linkage decreases when replacing In with smaller M (M = Mn, Ti, Zn, Al) cations in the selected purple series $YIn_{1-x}M_xO_3$ (Supporting Information Figure S3). Similarly, using smaller Ga^{3+} (0.55 Å) to replace some In^{3+} in $YIn_{1-x}Mn_xO_3$ can also shift the color from blue to violet or purplish blue, but the successful substitution is limited to $x \sim$ 0.1 by solid state synthesis. Adding more Ga to the hexagonal lattice would require a sol−gel precursor route that likely involves incorporation of carbonate groups into the crystal structure.[15,17]

The results of diffuse reflectance measurements are shown in Figure 7 and Supporting Information Figures S4−S6. White

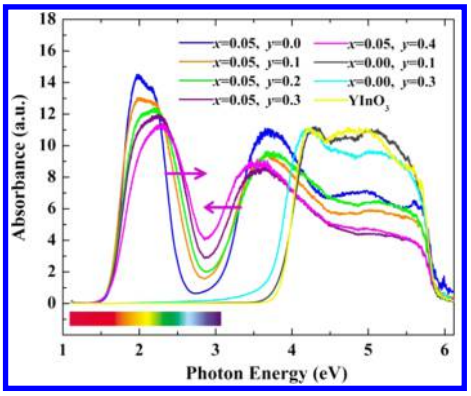

Figure 7. Diffuse reflectance spectra for selected purple samples $YIn_{1-x-2y}Mn_xTi_yZn_yO_3$ (x = 0.05, y = 0.1−0.4). Blue $YIn_{0.95}Mn_{0.05}O_3$, $YInO_3$, and compositions without the Mn chromophore (x = 0.00, y = 0.1 and 0.3) are included for comparison.

$YInO_3$ and $YIn_{1-2y}Ti_yZn_yO_3$ samples exhibit insignificant absorption across the entire visible range. For the purple solid solution $YIn_{1-x-2y}Mn_xTi_yZn_yO_3$ with increasing concentration of Ti/Zn, the lower-energy absorption peak is blue-shifted by 0.1−0.4 eV, and the onsets of the higher-energy absorption peak are red-shifted by 0.1−0.4 eV with respect to the blue. We assign the lower-energy absorption to the allowed d−d transition ($e'(d_{x^2-y^2}, d_{xy})$ to $a'(d_{z^2})$) as shown in Figure 1 and the absorption in the near-UV to a charge-transfer transition from O to Mn. These peaks also broaden because of the disorder around Mn with respect to In, Ti, Zn near neighbors. The color is defined by the minimum absorption, and that shifts to higher energy with increasing y. In comparison to blue $YIn_{0.95}Mn_{0.05}O_3$ the shorter Mn−O distances impact both the d−d transition and the charge-transfer peaks. It yields a larger ligand field splitting because it is mainly the apical Mn−O distance that decreases, which causes the d−d transition to move to a higher-energy range of the visible (from orange to yellow-green). Also, the Mn^{3+}−O^{2-} charge transfer becomes somewhat easier as the Mn−O distance decreases; consequently, the associated higher-energy absorption band moves to lower-energy range. These two effects induced by the shorter Mn−O distances give rise to a slight increase in the absorption at the bottom of the valley (~2.7 eV). The same valley also rises in blue series $YIn_{1-x}Mn_xO_3$ with an increasing amount of Mn due to the Mn−Mn charge transfer ($2Mn^{3+} \rightarrow Mn^{2+} + Mn^{4+}$) not shorter Mn−O distances.[1] This is not as obvious in the purple $YIn_{1-x-2y}Mn_xTi_yZn_yO_3$ ($x \leq 0.2$) series due to the low Mn content. The impact of Y-site substitution upon optical absorption is almost negligible (Supporting Information Figures S5−S6).

We also characterized the hue (color), chroma (vividness/dullness), and brightness of our powder samples using the CIE $L^*a^*b^*$ color space. The results are shown in Table 1 and Supporting Information Figures S7−S8. The scheme of 3-dimentional CIE color space is illustrated in Figure S7, and experimental data for selected colors of $YIn_{1-x}M_xO_3$ (M = Mn,

DOI: 10.1021/acs.inorgchem.6b01639
Inorg. Chem. 2016, 55, 9798−9804

Table 1. CIE $L^*a^*b^*$ Values of $YIn_{1-x-2y-z}Mn_xTi_yZn_yAl_zO_3$ (x = 0.005)

y	z	$x + 2y + z$	L^*	a^*	b^*	color
0	0	0.005	55.92	2.2	−34.93	light blue
0.1	0	0.205	39.36	9.23	−37.15	violet
0.2	0	0.405	35.42	13.74	−34.61	purple
0.3	0	0.605	33.36	14.45	−21.39	purple
0.4	0	0.805	43.81	15.27	−17.26	reddish purple
0.2	0.1	0.505	50.82	17.28	−24.52	purple

Fe, Cu/Ti, Mn/Ti/Zn) solid solutions are graphically represented. A unique color can be described precisely by 3-dimensional color coordinates L^*, a^*, and b^*. The vertical axis L^* gives the brightness from 0 (black) to 100 (white). The value of a^* shows colors from green to red (− to +) and b^* from blue to yellow (− to +) with neutral gray values at $a^* = 0$ and $b^* = 0$. A quantification of the colors for the $YIn_{1-x-2y-z}Mn_xTi_yZn_yAl_zO_3$ (x = 0.005) solid solution is reported in Table 1 and compared with the x = 0.05 series in Supporting Information Figure S8. When Mn content is low (x = 0.005), an increase of positive a^* values with Ti/Zn in the $+a$ direction is observed, depicting a shift toward red. At the same amount of Ti/Zn, replacing a little extra Al^{3+} (z = 0.1) for In^{3+} adds more reddish hue (Table 1) likely due to even shorter Mn−O apical distances close to the smallest Al^{3+} (0.48 Å). Along the b^* axis, negative b^* values move in the $+b$ direction regardless of Mn concentration, representing a shift toward yellow with increasing Ti/Zn (Figure S8). In general, going from blue to purple, the color appears slightly duller or less vivid (i.e., moving from the perimeter to center) as shown in Supporting Information Figure S7 with larger or similar brightness.

In addition to color, another desired property of pigments is the ability to reflect heat. This is becoming especially important due to rising energy costs. Near-infrared (NIR) energy contributes to ∼52% of the total solar radiation absorbed by earth as heat. White pigments like TiO_2 can reflect more than 80% of NIR radiation, leading to less NIR absorption, less heat build-up, and hence less cooling expense. However, there is high demand for colors other than white, including dark colors, that still have heat-reflective properties (i.e., "cool pigments"). Our NIR measurements in the range 700−2500 nm show unusually high reflectance for all the purple $YIn_{1-x-2y-z}Mn_xTi_yZn_yAl_zO_3$ ($x \le 0.2$, $y \le 0.4$, and $z \le 0.1$) samples synthesized in this work (Figure 8). Despite the amount of Ti/Zn and Al,

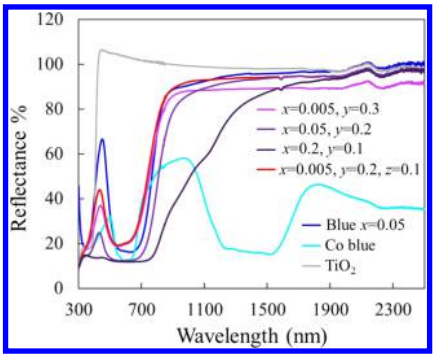

Figure 8. Vis−NIR reflectance spectra of selected purple $YIn_{1-x-2y-z}Mn_xTi_yZn_yAl_zO_3$ samples. Blue $YIn_{0.95}Mn_{0.05}O_3$, commercial Co blue, and TiO_2 are shown for comparison.

purple samples with low Mn content show ∼90% reflectance across the entire NIR range, just like the blue $YIn_{0.95}Mn_{0.05}O_3$. This value drops gradually with increasing Mn between 700 and 1500 nm, but is still much higher than that of the Co-based pigment from 1100 to 2500 nm as shown in Figure 8. The excellent NIR reflectance that is comparable to TiO_2 makes this purple pigment a potential candidate for many applications where solar heat reflection and energy-saving properties are desired.

To confirm the presence of Mn^{3+}, we conducted the magnetic susceptibility measurements. The temperature dependence of the magnetic susceptibility (χ) and inverse magnetic susceptibility ($1/\chi$) for selected purple samples are shown in Figure 9. The susceptibility χ increases rapidly below

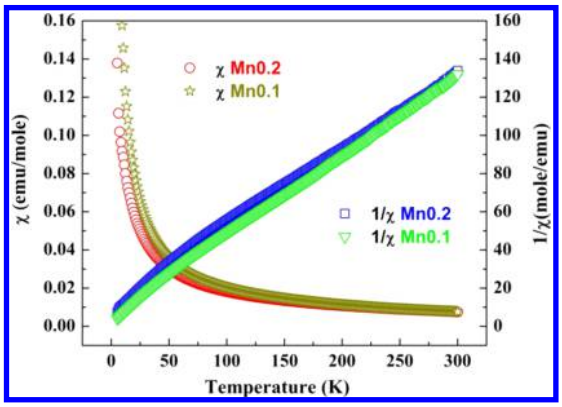

Figure 9. Temperature dependence of the magnetic susceptibility (χ, 1 emu $=10^{-3}$A m^2) and inverse magnetic susceptibility ($1/\chi$) for selected purple sample $YIn_{0.4}Mn_{0.2}Ti_{0.2}Zn_{0.2}O_3$ (Mn0.2) and $YIn_{0.6}Mn_{0.1}Ti_{0.1}Zn_{0.1}Al_{0.1}O_3$ (Mn0.1). Calculated Curie constant C and Weiss constant θ_w are C = 2.57, θ_w = −40.3 for Mn0.2 and C = 2.38, θ_w = −11.5 for Mn0.1, respectively.

50 K, indicating increased spin alignment in response to applied magnetic field. The Curie−Weiss law, $\chi = C/(T - \theta_w)$, is obeyed on the basis of the observed linear trend of $1/\chi$ versus T in the high-temperature region. The values of Curie constant C and Weiss constant θ_w are determined from the paramagnetic region (150−300 K) of the inverse susceptibility by fitting the linear portion. The obtained negative Weiss constant is indicative of antiferromagnetic behavior being dominant. At lower Mn concentration, the Weiss constant is less negative as Mn−Mn interaction becomes weaker, especially as Mn−O−Mn linkages disappear (Figure 9). The effective magnetic moments, μ_{eff}'s, for selected $YIn_{1-x-2y-z}Mn_xTi_yZn_yAl_zO_3$ samples are 4.38 μ_B ($x = y = z$ = 0.1) and 4.55 μ_B ($x = y$ = 0.2, z = 0), respectively, calculated from the obtained Curie constants. These values are close to the theoretical magnetic moment, μ_{th} = 4.90 μ_B, for high-spin Mn^{3+} ($3d^4$), supporting the existence of trivalent Mn in these hexagonal oxides. Previously, EPR was also utilized to confirm Mn^{3+} in $YIn_{1-x}Mn_xO_3$ phases.[29]

In addition to its color and heat-reflective properties, thermal and chemical stability is a desirable property for a pigment, and this is not the case for several commercial violet/purple pigments. Cobalt Violet ($Co_3(PO_4)_2$), Manganese Violet ($NH_4MnP_2O_7$), and Ultramarine Violet ($Na_{10}Al_6Si_6O_{24}S_4$) decompose at fairly low temperatures (<500 °C), and some change color or even dissolve under acidic conditions. Furthermore, the manufacture of ultramarine involves SO_2

DOI: 10.1021/acs.inorgchem.6b01639
Inorg. Chem. 2016, 55, 9798−9804

emission, and the toxicity of cobalt is of concern in the preparation and application of pigments. We performed heating and acid tests on our well-characterized purple pigments. The synthesis temperature is ∼1300 °C, but these pigments can endure even higher temperatures while maintaining their original colors. Treating our pigments with 10∼50% of HNO_3, HCl, or H_2SO_4 solutions and stirring overnight resulted in negligible weight and color changes, and XRD patterns remain the same after the tests. With their unprecedented NIR reflectance and stability against heat and acids, our environmentally benign violet/purple pigments may find wide applications in the coloration of high-performance plastics and coatings, building exteriors, cool roofing, vinyl siding, automobiles, and even art restoration where highly durable and/or cost-effective energy-saving pigments are preferred.

CONCLUSIONS

We demonstrate with the $YInO_3$−$YMnO_3$ system that colors can be designed by manipulating the crystal structure, in this case the local environment of the Mn^{3+} chromophore in trigonal bipyramidal coordination. Our novel nontoxic violet/purple pigments surpass the existing synthetic pigments in durability, thermal stability, NIR reflectance, and hence energy-saving properties. The lower indium content due to Ti/Zn/Al substitution reduces the cost of the pigments, and the simple preparation via solid state reaction offers advantages for industrial manufacturing process in contrast with the solution routes of some existing purple pigments. We expect that our results may lead to routes for the development of inexpensive, earth-abundant based, environmentally benign, and highly stable inorganic pigments.

ASSOCIATED CONTENT

Supporting Information

The Supporting Information is available free of charge on the ACS Publications website at DOI: 10.1021/acs.inorgchem.6b01639.

Additional figures, including XRD data, spectra, and CIE information (PDF)

Crystallographic data (CIF)

AUTHOR INFORMATION

Corresponding Author

*E-mail: mas.subramanian@oregonstate.edu.

Notes

The authors declare no competing financial interest.

ACKNOWLEDGMENTS

This work was supported by NSF Grant DMR 1508527. The identification of any commercial product or trade name does not imply endorsement or recommendation by the National Institute of Standards and Technology.

REFERENCES

(1) Smith, A. E.; Mizoguchi, H.; Delaney, K.; Spaldin, N. A.; Sleight, A. W.; Subramanian, M. A. Mn^{3+} in Trigonal Bipyramidal Coordination: A New Blue Chromophore. *J. Am. Chem. Soc.* **2009**, *131*, 17084−17086.

(2) Chang, K. By Happy Accident, Chemists Produce a New Blue. *The New York Times* **2009**, No. Nov 24, D3.

(3) Stone, D. Coat d'Azure. *Natl. Geogr.* **2013**, *223* (2), 19.

(4) Ball, P. Blues Standard. *Chemistry World* Sept 27, **2012**.

(5) Jiang, P.; Li, J.; Sleight, A. W.; Subramanian, M. A. New Oxides Showing an Intense Orange Color Based on Fe^{3+} in Trigonal-Bipyramidal Coordination. *Inorg. Chem.* **2011**, *50*, 5858−5860.

(6) Smith, A. E.; Sleight, A. W.; Subramanian, M. A. Synthesis and Properties of Solid Solutions of Hexagonal $YCu_{0.5}Ti_{0.5}O_3$ with YMO_3 (M = Mn, Cr, Fe, Al, Ga, and In). *Mater. Res. Bull.* **2011**, *46*, 1−5.

(7) Varichon, A. *Couleurs-Pigments dans les Mains des Peoples*; Éditions du Seuil: Paris, 2005; pp 133−146.

(8) Berke, H. The Invention of Blue and Purple Pigments in Ancient Times. *Chem. Soc. Rev.* **2007**, *36*, 15−30.

(9) Berke, H. Chemistry in Ancient Times: The Development of Blue and Purple Pigments. *Angew. Chem., Int. Ed.* **2002**, *41*, 2483−2487.

(10) Eastaugh, N.; Walsh, V.; Chaplin, T. *Pigment Compendium: A Dictionary and Optical Microscopy of Historical Pigments*; Routledge: Abingdon, 2008.

(11) Corbeil, M. C.; Charland, J. P.; Moffatt, E. A. The Characterization of Cobalt Violet Pigments. *Stud. Conserv.* **2002**, *47*, 237−249.

(12) Pavey, D. *Colour Concepts Palettes and Pigments*; Lulu.com: Raleigh, 2014; pp 223.

(13) Clark, R. J. H.; Dines, T. J.; Kurmoo, M. On the Nature of the Sulfur Chromophores in Ultramarine Blue, Green, Violet, and Pink and of the Selenium Chromophore in Ultramarine Selenium: Characterization of Radical Anions by Electronic and Resonance Raman Spectroscopy and the Determination of Their Excited-state Geometries. *Inorg. Chem.* **1983**, *22*, 2766−2772.

(14) Adem, U.; Nugroho, A. A.; Meetsma, A.; Palstra, T. T. M. Ferroelectric Displacements in Multiferroic $Y(Mn,Ga)O_3$. *Phys. Rev. B: Condens. Matter Mater. Phys.* **2007**, *75*, 014108.

(15) Tamilarasan, S.; Sarma, D.; Reddy, M. L. P.; Natarajan, S.; Gopalakrishnan, J. $YGa_{1-x}Mn_xO_3$: A Novel Purple Inorganic Pigment. *RSC Adv.* **2013**, *3*, 3199−3202.

(16) Li, J.; Singh, U. G.; Schladt, T. D.; Stalick, J. K.; Scott, S. L.; Seshadri, R. Hexagonal $YFe_{1-x}Pd_xO_{3-\delta}$: Nonperovskite Host Compounds for Pd^{2+} and Their Catalytic Activity for CO Oxidation. *Chem. Mater.* **2008**, *20*, 6567−6576.

(17) Li, J.; Smith, A. E.; Jiang, P.; Stalick, J. K.; Sleight, A. W.; Subramanian, M. A. True Composition and Structure of Hexagonal "$YAlO_3$", Actually $Y_3Al_3O_8CO_3$. *Inorg. Chem.* **2015**, *54*, 837−844.

(18) Mizoguchi, H.; Sleight, A. W.; Subramanian, M. A. New Oxides Showing an Intense Blue Color Based on Mn^{3+} in Trigonal-Bipyramidal Coordination. *Inorg. Chem.* **2011**, *50*, 10−12.

(19) Kim, T. G.; Kim, S. J.; Lin, C. C.; Liu, R. S.; Chan, T. S.; Im, S. J. Melilite-type Blue Chromophores Based on Mn^{3+} in a Trigonal-bipyramidal Coordination Induced by Interstitial Oxygen. *J. Mater. Chem. C* **2013**, *1*, 5843−5848.

(20) Saraswathy, D.; Rao, P. P.; Sameera, S.; James, V.; Raj, A. K. V. Monoclinic $LaGa_{1-x}Mn_xGe_2O_7$: A New Blue Chromophore Based on Mn^{3+} in the Trigonal Bipyramidal Coordination with Longer Apical Bond Lengths. *RSC Adv.* **2015**, *5*, 27278−27281.

(21) Larson, A. C.; Von Dreele, R. B. *General Structure Analysis System (GSAS) Report LAUR 86-748*; Los Alamos National Laboratory: Los Alamos, 2004.

(22) Toby, B. H. EXPGUI, A Graphical User Interface for GSAS. *J. Appl. Crystallogr.* **2001**, *34*, 210−213.

(23) Hormillosa, C.; Healy, S.; Stephen, T.; Brown, I. D. *Bond Valence Calculator [Online], version 2.0*; 1993. http://www.ccp14.ac.uk/ccp/web-mirrors/i_d_brown/ (accessed Aug 12, 2016).

(24) Kubelka, P.; Munk, F. Ein Beitrag zur Optik der Farbanstriche. *Z. Technol. Phys.* **1931**, *12*, 593−601.

(25) Bain, G. A.; Berry, J. F. Diamagnetic Corrections and Pascal's Constants. *J. Chem. Educ.* **2008**, *85*, 532−536.

(26) Li, J.; Sleight, A. W.; Subramanian, M. A. Determination of the Local Environment of Mn^{3+} and In^{3+} in the $YInO_3$-$YMnO_3$ Solid Solution, Which Exhibits an Intense Blue Color. *Chem. Mater.* **2016**, DOI: 10.1021/acs.chemmater.6b02827.

(27) Shannon, R. D. Revised Effective Ionic Radii and Systematic Studies of Interatomic Distances in Halides and Chalcogenides. *Acta*

DOI: 10.1021/acs.inorgchem.6b01639
Inorg. Chem. 2016, 55, 9798−9804

Crystallogr., Sect. A: Cryst. Phys., Diffr., Theor. Gen. Crystallogr. **1976**, *A32*, 751−767.
(28) Pistorius, C. W. F. T.; Kruger, G. J. Stability and Structure of Noncentrosymmetric Hexagonal $LnInO_3$ (Ln = Eu, Gd, Tb, Dy, Ho, Y). *J. Inorg. Nucl. Chem.* **1976**, *38*, 1471−1475.
(29) Krzystek, J.; Telser, J.; Li, J.; Subramanian, M. A. Magnetic Properties and Electronic Structure of Manganese-Based Blue Pigments: A High-Frequency and -Field EPR Study. *Inorg. Chem.* **2015**, *54*, 9040−9045.

DOI: 10.1021/acs.inorgchem.6b01639
Inorg. Chem. 2016, 55, 9798−9804